Leibniz-Gemeinschaft

Final report

Title of the project:

Mapping nonequilibrium electron density distributions in space and time by femtosecond x-ray diffraction

Leibniz-Institute: Max Born Institute
Reference number: SAW-2014-MBI-1
Project period: 01.01.2014 – 31.12.2016
Contact partner: Dr. Uwe Griebner / Prof. Thomas Elsässer

Executive Summary

The study of x-ray scattering and diffraction methods for determining the structure of atoms, molecules, and/or their periodic arrangement in crystals benefits substantially from the development of kilohertz repetition rate few-cycle optical driver pulses at mid-infrared (mid-IR) wavelengths. Optical parametric chirped pulse amplification (OPCPA) pumped by a highly stable, picosecond pump sources near 2 μm is an energy-scalable approach for generating the required driver pulses for this and other applications. The main objective of the project was the development of a mid-IR OPCPA system providing few-cycle pulses at 5 μm at a pulse energy level beyond the contemporary state of the art mid-IR sources at a repetition rate of 1 kHz. The target, sub-100 fs pulses at a >1-mJ pulse energy and a center wavelength of 5 μm was to be achieved, on the basis of a 2-μm pump pulse source, in order to push the existing technological limits and widen the application range of OPCPA systems.

The developed picosecond 2-μm pump source is based on optical amplification in Ho:YLF and delivers 55 mJ pulses at a 1 kHz repetition rate, to the best of our knowledge the highest pulse energy reported for kHz CPA systems at 2 μm. The system, operating at room temperature, displays an excellent stability with a pulse-to-pulse rms as low as 0.3%. This low noise level mainly originates from a high-gain Ho:YLF regenerative amplifier (RA), which is optimized for stable operation in the single-energy regime. In a 1 kHz pulse train, ~10 mJ pulses were generated, the highest energy to date of any single-energy picosecond RA emitting around 2 μm. Seeding the two subsequent single-pass booster amplifiers a single pass gain of 5.8 was achieved, resulting in 55 W average power. This value corresponds to a high extraction efficiency for the whole amplifier system beyond 20% with respect to the optical pump power. Pulse compression at 25 mJ pulse energy provides almost transform-limited pulses with a duration of 4.3 ps, translating into the highest peak power of 4.4 GW achieved for 2-μm CPA systems so far. The 2-μm source is used to pump the mid-IR OPCPA to exploit the high nonlinearity of $ZnGeP_2$ crystals for parametric amplification. The 5-μm OPCPA system delivers multi-GW femtosecond pulses at a 1 kHz repetition rate. In the 1 kHz pulse train, up to 1.3 mJ idler pulses were generated and compressed to 160 fs duration by dispersion management based on bulk materials only. This pulse duration corresponds to a sub-ten cycle signature. After optimizing the higher-oder dispersion in the OPCPA chain, 75 fs pulses at a 0.65 mJ energy were demonstrated. The pulse energy represents the highest to date of any femtosecond mid-IR source beyond 4 μm. The OPCPA is characterized by an excellent stability with a pulse-to-pulse rms as low as 1.3%. This pulse characteristics represents the highest peak power of 5.3 GW achieved for 5-μm OPCPA systems to the best of our knowledge, and, if focused to a 15-μm spot diameter, would reach a peak intensity of ~6×10^{15} W/cm^2.

Based on the existing system, further scaling of the 5-μm pulse energy is straightforward using the remaining 2-μm pump power. Furthermore, the system appears scalable with respect to repetition rate via a pulse picking rate in the 1 to 10 kHz range. This will lead to hitherto inaccessible pulse energies and peak intensities paving the way for a deeper understanding of the relation between structural and functional properties of matter.

Table of Contents

1. Objectives

This proposal aimed at developing, implementing, and applying experimental infrastructure for determining transient electron density maps in crystals with a spatial resolution of 0.01 nm and a temporal resolution of 100 fs. The key components are (i) a tabletop optical driver system providing 5 mJ sub-50 fs pulses at a 5 µm wavelength with a 1 kHz repetition rate, (ii) a hard x-ray plasma source implementing copper or molybdenum targets, and (iii) a setup for x-ray powder diffraction to record diffraction patterns consisting of several tens of reflections.

2. Results

The description of the results follows the project plan and work packages (WPs) as listed in the project proposal. The basic layout of the mid-IR driver system was implemented as originally planned in the proposal. At first, the implementation of the three main components of the OPCPA system, the seed source, the 2-µm pump chain and the OPCPA stages will be discussed in detail. Then, the route for the implementation of the mid-IR driver source for x-ray generation will be discussed.

2.1 Seed source for the OPCPA and the 2-µm pump laser

As the front-end seed laser, a commercial, multi-color Er:fiber laser system (Toptica) is used to provide optically synchronized pulses at 1.0 µm and 1.5 µm for the DFG and 2.0-µm for the pump beam of the OPCPA (Fig. 1). The master module operating at 1.5 µm contains a 40-MHz oscillator, an amplifier and a Si prism compressor. The two slave modules are supercontinuum (SC) modules, which are seeded from the master module and contain only amplifiers, prism compressors, and a highly nonlinear fiber (HNLF). The pulses were characterized using a home-built autocorrelator. Accordingly, it was determined that 75-fs pulses were provided directly from the master module at 1.5 µm, 600 fs pulses from the 2.0 µm SC output in the spectral range of interest, and 15 fs at 1.0 µm after compression of the respective SC output by a pair of chirped mirrors. The long term stability was found to be limited by the stability of the ambient temperature, as the temperature of the modules were not actively stabilized. Furthermore, a warm-up time of >6 hours was needed to reach a stable spectral emission of the three arms.

2.2 Selection of the gain medium for the 2-µm amplifier chain

Suitable OPCPA sources at longer mid-IR wavelengths require adequate pump laser systems which work at wavelengths above 2 µm with kilohertz repetition rates and provide pulse durations of up to several tens of picoseconds. Ho-based amplifiers seeded by picosecond pulses appear well suited to pump OPCPA schemes operating in the few-cycle regime beyond 4 µm wavelength [1]. Among the 2-µm laser gain media, Ho-doped materials offer long upper-state lifetimes as well as high stimulated-emission cross sections, which render them favorable for obtaining high-repetition rate, high-energy pulses.

At kilohertz repetition rates close to the inverse upper state lifetime of Ho, one enters an operation regime in which continuously pumped regenerative amplifiers (RAs) can display energy instability and/or a multistable output energy [2]. This issue, a key problem for any application of RAs in experiments, is addressed in a systematic and quantitative way in chapter 2.3. The selection of the particular active 2-µm amplifier material was performed at a higher repetition rate of 10 kHz where bifurcation instabilities play a minor role.

The layout of the 2-µm seed source and the regenerative amplifier (RA) is shown in Fig. 1 and consists of four main parts, (i) a supercontinuum seed source, (ii) a Tm:fiber pre-amplifier (AdValue), (iii) a pulse stretcher and (iv) the RA. The supercontinuum is generated in a highly nonlinear fiber (HNLF) by launching the 75 fs pulses at 1.55 µm from the Er:fiber oscillator/power amplifier. The HNLF output encompasses the spectral range 1.8 – 2.4 µm at an average power of 48 mW. A single-stage Tm:fiber amplifier suffices to pre-amplify the supercontinuum pulses. This pre-amplifier is designed to support the spectral range from 2040 to 2100 nm in which the peak gain wavelengths of the most favorable Ho-transitions are located [3]. The input pulses are negatively chirped, permitting amplification in fiber-based

systems in the anomalous regime without risk of nonlinear phase distortion and avoiding collapse or self-compression. They experience temporal stretching during amplification from the negative group delay dispersion (GDD) of the Tm-doped fiber. The pre-amplified pulses reach 18 nJ in energy at a 9 ps duration with a GDD of -0.85 ps^2. Figure 2(a) (black solid line) shows their spectrum extending from 2030 to 2110 nm (zero level).

After pre-amplification, the pulse train passes a pulse picker (RTP) and an optical isolator. The former reduces the 40 MHz repetition rate to 1-10 kHz. Subsequently, pulses are stretched to ~400 ps using a double-pass in a 600 line/mm reflective Treacy-type grating arrangement with a total GDD of –35 ps^2. Because of reflection losses, the stretched pulses have a reduced total energy of 2 nJ. Although this setup does not permit shaping at high spectral resolution, blocking of undesired spectral segments apparently suffices for suppressing spectral sidebands and for avoiding pre- or post-pulses.

The design of the regenerative amplifier (RA) is based on a ring cavity because of its proven stability against changes of pump power and resulting changes of the thermal lens (Fig. 1). This approach which was also applied in [4,5] allows the implementation of two thin-film polarizers for separating input and output ports. A Faraday rotator as typically used in a linear cavity, is not necessary here and was omitted. The ring resonator is formed by 6 highly reflecting mirrors and requires operation of an RTP Pockels cell (Leysop) in the λ/2 regime, in combination with a half-wave plate. As active media, we employ 50 mm long antireflection-coated Ho-doped rods, which are end-pumped by an unpolarized cw Tm:fiber laser at 1940 nm (IPG Photonics) and directly water-cooled to room temperature.

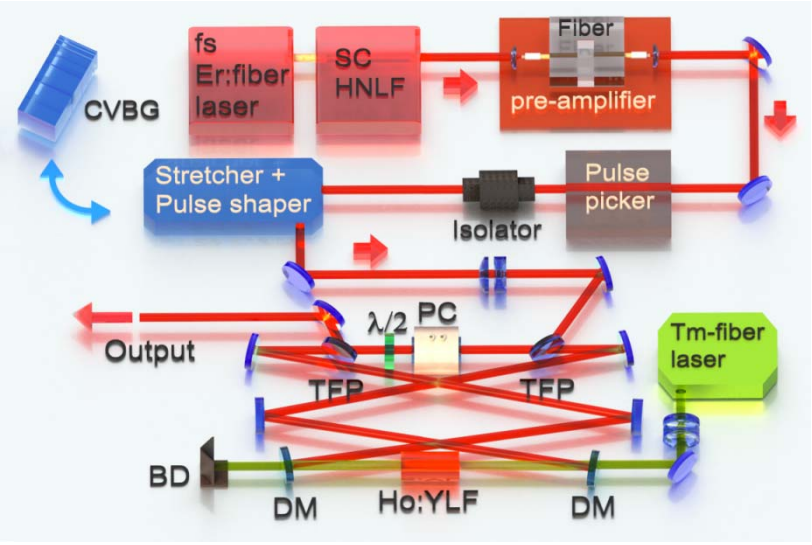

Fig. 1. Setup of 2-µm CPA system containing a supercontinuum seed source, single stage fiber pre-amplifier, grating based stretcher with pulse shaper, and the cw-pumped RA. SC, supercontinuum generation; HNLF, highly nonlinear fiber; PC, Pockels cell; TFP, thin-film polarizer; λ/2, half-wave retarder; Ho:YLF, gain media.

Our study focuses on the birefringent Ho:YLF as a gain medium, given its ~5-times lower nonlinearity as well as its lower and negative thermal change of refractive index dn/dT in comparison to the isotropic Ho:YAG [6]. In contrast, Ho:YAG emits at longer wavelengths and may therefore appear preferable over Ho:YLF for pumping OPCPA, granted the weaker residual absorption in $ZnGeP_2$, which has been favorably employed for mid-IR OPAs [7]. The emission cross sections for E∥c and E⊥c in Ho:YLF are given as inset in Fig. 2(a) [8]. The measured single pass gain spectra of Ho:YLF (E∥c) and Ho:YAG when seeded with our supercontinuum source are included in Fig. 2(b).

Given the targeted high repetition rate and single-energy performance, the RA is operated at 10 kHz. Initially we inserted a 0.5% Ho-doped YLF crystal in E∥c orientation (π-polarization) in

the RA, in order to benefit from the maximum gain cross section at 2050 nm [8]. The seed spectrum was spectrally shaped to suppress the gain peak at 2060 nm (Fig. 2(a), red horizontal bar), resulting in a seed energy of ~0.15 nJ.

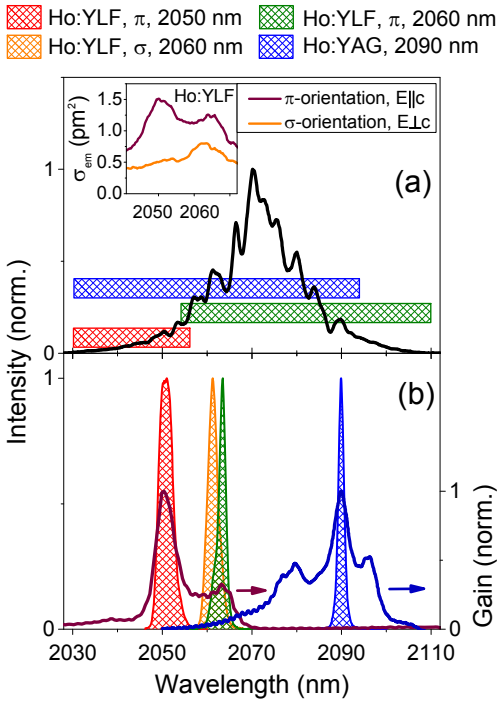

Fig. 2. (a) Pulse spectrum after the single-stage Tm:fiber pre-amplifier (solid line). Color coded bars: shaped seed spectra for operating RA at 2050 nm (red), 2060 nm (green) or 2090 nm (blue). Inset: emission cross sections (σ_{em}) of Ho:YLF at room temperature for E∥c and E⊥c. (b) Pulse spectra of the studied Ho:YLF and Ho:YAG RAs at maximum pump power (shaded profiles) and measured gain spectra of Ho:YLF (E∥c) and Ho:YAG at 15 W pump power when seeded with our supercontinuum source (brown and blue curves).

Figure 3(a) shows the pulse energy versus pump power for the RA's investigated. At 2050 nm, the highest pulse energy of 1.1 mJ is achieved for the Ho:YLF RA operating with 24 round trips (Fig. 3(a), red squares). The pulse energy corresponds to a net gain of ~10^7 and yields the maximum average power of 11 W. Taking into account the applied pump power of 48 W this corresponds to a sizeable optical-to-optical efficiency of 23%. The linear dependence in Fig. 3(a) verifies the calculated continuous tunable energy scaling. Since no saturation occurred during amplification at this energy level, output energies appear further scalable. However, the analysis of the pulse-to-pulse stability at 1.1 mJ as compared to <1.0 mJ indicate a slight but significant increase of pulse energy fluctuations. Thus, the 1.1 mJ pulse energy value marks the limit of the tunable single-energy regime and corresponds to the first bifurcation point of our system. As a consequence, only further average power scaling in the tunable single-pulse regime is possible for which the repetition rate has to be increased. The generated spatial beam profile exhibits TEM_{00} characteristics with M^2 <1.2 (Fig. 3(a), inset). The resonator arrangement ensures spatial mode stability over the whole pump power range without need for compensation of thermal effects. At a reduced pulse repetition rate, the onset of periodic double pulsing and chaotic behavior starts at a substantially lower power level. In the case of 5 kHz this level is reached in our RA at about 32 W pump power.

Spectra of the amplified pulses summarized in Fig. 2(b). For the present Ho:YLF (E∥c) case with a 2050 nm seed (red bar in Fig. 2(a)), the spectrum of the amplifier output has its maximum at 2051 nm with a spectral width (FWHM) of 3.2 nm (red contour in Fig. 2(b)). Ho:YLF exhibits a second gain maximum at 2060 nm with lower gain for the same polarization orientation parallel to the c-axis (E∥c) (Fig. 2(a), inset). Tailoring the spectrum of the input

pulses fed into the RA allows for changing the spectral position of the amplified pulses. Amplified pulses centered at 2062 nm are readily generated with input pulses of 0.7 nJ energy taking into account the gain spectrum (Fig. 2(b)) and the seed spectral range between 2055 and 2110 nm (green horizontal bar in Fig. 2(a)). Compensating the lower gain around 2060 nm by increasing the number of round-trips from 24 to 33, we generated similar pulse energies up to 0.95 mJ at a 10 kHz repetition rate with nearly the same slope efficiency (Fig. 3(a)). The recorded emission spectrum for the E∥c orientation displays a spectral bandwidth of 1.7 nm (FWHM, green profile in Fig. 2(b)), mostly limited by gain narrowing in the Ho:YLF RAs.

So far, all demonstrated Ho:YLF power amplifiers operated in single-pass arrangements at 2050 nm (E∥c) because of the very low gain at this wavelength for E⊥c orientation (inset, Fig. 2(a)). At 2060 nm, in contrast, the spectral position and the peak emission cross section are nearly identical for both orientations (Fig. 2(a), inset). As shown in Fig. 3(a), amplification for the σ-polarization (E⊥c) at 2060 nm is only slightly reduced compared to E∥c, resulting in maximum pulse energies of 0.91 mJ. The emission spectrum exhibits a bandwidth of 2.1 nm (orange profile in Fig. 2(b)). Single-rod Ho:YLF double-pass power amplifiers at 2060 nm are, thus, an option, and a reduced gain narrowing is expected because of the slightly displaced peak wavelengths of ~1.5 nm (Fig. 2(b)).

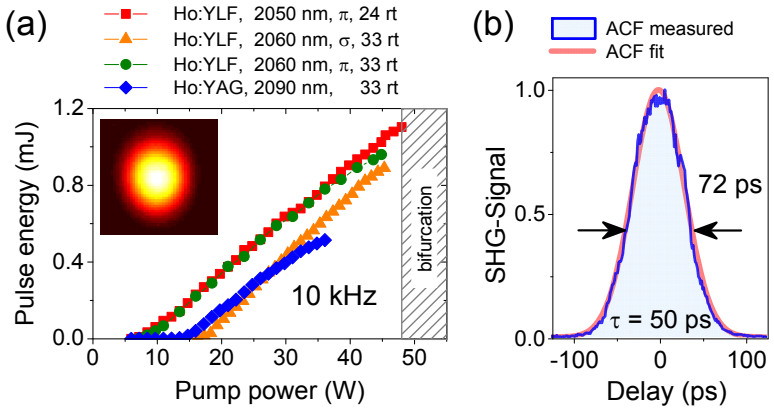

Fig. 3. (a) Dependence of output pulse energy on pump power of the Ho:YLF and Ho:YAG RAs at 10 kHz (shaded area: region of the first bifurcation point (S_1, Fig. 4a), rt: round trips). Inset: far-field beam profile. (b) Typical autocorrelation trace (ACF) of the Ho:YLF RAs. Fits assume Gaussian pulses.

The pulse duration for the Ho:YLF RAs was measured at maximum pulse energy with a commercial autocorrelator (APE). We find a value of ~50 ps (Fig. 3(b)) which appears well suited for pumping OPCPAs. In principle, the spectra support minimum pulse duration of ~2 ps, requiring a recompression of the RA output.

Finally, a 1% Ho-doped YAG rod was tested in our RA operating at 2090 nm. Applying the same procedure as described above, the seed spectrum was shaped to suppress the 2097 nm line (Fig. 2(a), blue horizontal bar). The energy of the seed pulse was 0.7 nJ. From the output characteristics at a 10 kHz repetition rate (blue symbols in Fig. 3(a)), one expects a performance similar to the Ho:YLF RA. We, however, limited the maximum pulse energy to 0.5 mJ to prevent any damage, given the much stronger gain narrowing compared to Ho:YLF. This precaution is confirmed by the narrower emission bandwidth of 1.2 nm (FWHM, blue profile in Fig. 2(b)) and the concomitant shorter pulse duration of 25 ps.

To summarize this chapter, pulse energies as high as 1.1 mJ were generated at 2050 nm by designing a high-gain, broadband seeded, cw-pumped Ho-doped RA which incorporates CPA. The demonstrated average power exceeds 10 W, corresponding to a remarkable optical-to-optical efficiency beyond 20%. The developed broadband seed source enables operation of RAs in the spectral range between 2050 – 2100 nm, encompassing most of the 2 µm Ho-transition. Despite an exceptional high net gain ~10^7 of the RA, no indication for a background was detected down to an energy level of 10^{-7}. The achieved output parameters of the RAs are

consistent with our simulations, indicating the onset of instabilities for pulse energies >1.1 mJ. The system appears scalable with respect to pulse energy. However due to the obtained strong gain narrowing temporal stretching of the pulses to well beyond 100 ps is required. Ho:YLF exhibits a much lower gain narrowing due to its lower nonlinear refractive index compared to Ho:YAG [4] and is therefore selected as gain material for the 2-µm amplifier chain.

2.3 Regenerative amplifier - overcoming bifurcation instability in few kHz repetition-rate 2 µm Ho-doped regenerative amplifiers

As mentioned in chapter 2.2, in continuous-wave (cw) pumped RAs, the amplified pulse train is influenced by gain depletion induced by the previous pulse, in particular when operating at repetition rates close to or higher than the inverse of the gain relaxation time [2]. Due to the incomplete gain recovery, fairly complex behavior may appear here, which ranges from period doubling to chaotic behavior. Previous reports on this rather undesired mode of operation exist in the literature, which, however, exclusively address the 1-µm spectral range [9]. Given the roughly tenfold shorter upper state lifetime τ_f of Nd- and Yb-doped gain media at 1 µm compared to Tm- and Ho-doped media at 2 µm, the region of bifurcation starts at significantly higher RA repetition rates, typically above ~5 kHz and ~1 kHz for Nd- and Yb-doped materials, respectively [2]. For the Ho:YLF gain medium emitting at 2.050 µm, however, this limit occurs at a much lower repetition rate of approximately 0.1 kHz (t_f = 14 ms). As the targeted repetition rates of our Ho:YLF RA are a few kHz, we performed a careful analysis of the deterministic chaos region during pulse amplification.

Our model is based on a modified Frantz-Nodvik equation [10] and takes into account the spectral features of the Ho:YLF gain medium and its quasi-three-level behavior. We consider a rotational symmetric amplifier with fixed pump- and laser-mode diameter which is end-pumped from one side at 1.940 µm. This wavelength corresponds to the $^5I_8 \rightarrow {}^5I_7$ transition in the Ho ion. The rate equations for the local population densities of the Ho manifolds are described according to [11]. We did not introduce the total upconversion loss constant [12], given that it can be neglected for the applied Ho dopant level of 0.5% in the YLF crystal [13]. The absorption and emission cross sections of Ho:YLF can also be found in Ref. 15 and the maxima amount to 1.02 x 10^{-20} cm^2 at 1940 nm and 1.50 x 10^{-20} cm^2 at 2050 nm, respectively for π-polarization. The temperature dependent Boltzmann population distribution functions of the two Ho manifolds are implemented as in [14].

The pump and amplification phase are calculated in sequence as the contribution to the inversion build-up by the pump is negligible during the amplification phase. In the pump phase, the propagating pump field and the inversion evolution are iterated along the axis of the amplifier rod (*z*-direction). For that case, the crystal rod with length *l* is split into a total number of m slices with thickness δz,

Simulation results of output pulse energy vs. incident pump power are shown in Fig. 4 for repetition rates of (a) 1 and (b) 2 kHz. To ensure steady-state operation, the simulation is executed with 150 pulses from a pulse train for each level of incident pump power. For the generation of the bifurcation diagrams, the pulse energy values for the last 50 pulses are plotted. Input parameters are chosen to match our seed source, which delivers broadband pulses with energies of about 2 nJ. The input pulses make 24 cavity round trips in the RA. For the sake of clarity we first consider the 2 kHz operation (Fig. 4b). The amplification threshold is reached at ~7 W of pump power, followed by a very narrow region $\mathbf{S_1}$ that is characterized by a linear increase of single-pulse energy with pump power up to ~1 mJ. After this first bifurcation point, a period-doubling cascade $\mathbf{P_1}$ starts, followed by a region χ_1 of irregular behavior. Further increase of pump power leads to an intermediate stable regime $\mathbf{P_2}$, succeeded by yet another irregular area χ_2, which is again followed by periodic doubling $\mathbf{P_3}$. Finally a second single-pulse energy regime $\mathbf{S_2}$ appears above 55 W pump power. This transition denotes the major final bifurcation point (BP_{final}) beyond which any multi-stabilities and chaotic behavior have been overcome.

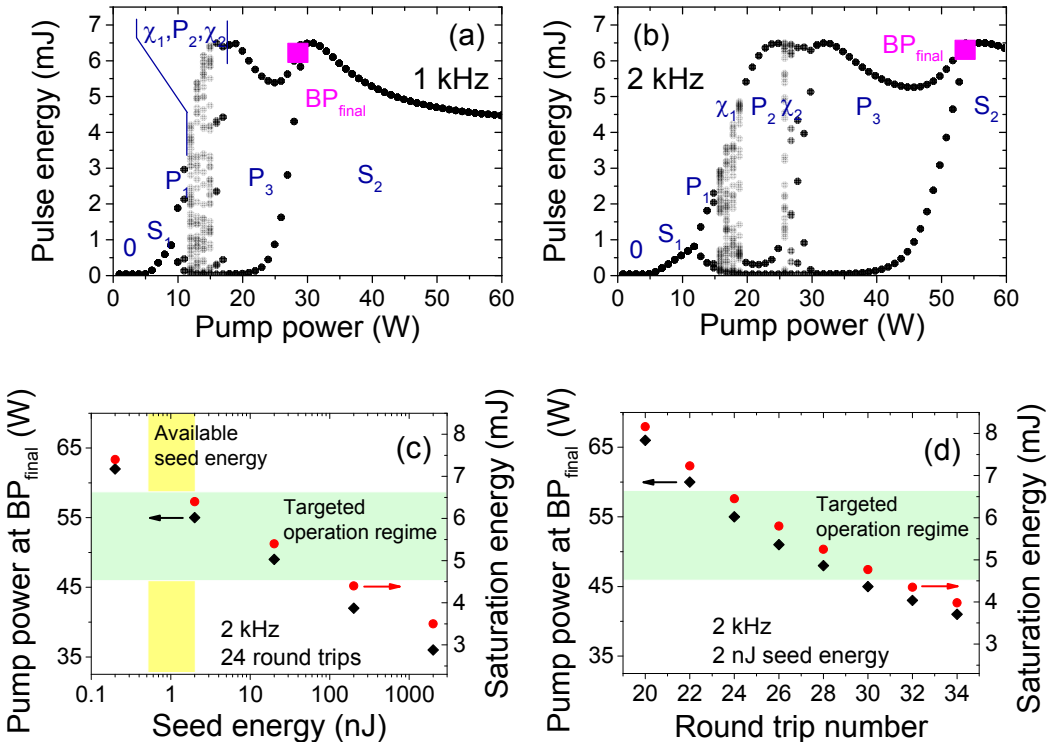

Fig. 4. Simulated pulse energy in dependence on the incident pump power of our cw pumped Ho:YLF RA assuming a constant mode diameter at repetition rates of (a) 1 kHz and (b) 2 kHz (round trips: 24, seed energy: 2 nJ). The labels **0**, $\mathbf{S_i}$, $\mathbf{P_i}$ and $\boldsymbol{\chi_i}$ mark the different characteristic regions in the bifurcation diagram and are explained in the text. BP_{final} marks the final bifurcation point where the system turns into the saturated single-energy regime $\mathbf{S_2}$. (c) Seed energy required for operation in the saturated single-energy regime $\mathbf{S_2}$ (crossing BP_{final}) and the corresponding pulse energy (24 round trips). (d) Influence of the round trip number for operation in the saturated single-energy regime $\mathbf{S_2}$ (crossing BP_{final}) and the corresponding pulse energy (seed energy: 2 nJ). Ho:YLF parameters: emission at 2050 nm, π-pol. (E||c).

Reducing the fundamental repetition rate to 1 kHz (Fig. 4a), a significant shift of the various characteristic regions along the pump power axis is observed. More importantly, the true single-pulse regime $\mathbf{S_2}$ already appears at lower pump powers above 30 W. For optimum energy extraction and pulse-to-pulse stability, amplifier saturation is required. Saturation with a pulse energy of 6.5 mJ is reached at a pump power of about 15 W and 22 W at 1 kHz and 2 kHz repetition rate, respectively.

It is important to note that variation of the number of round trips for a fixed repetition rate and seed energy changes the extension of the characteristic regions and the scaling on the pump power axis [2]. In the single-energy region $\mathbf{S_1}$ below the first bifurcation point, however, only a weak dependence on seed pulse energy between 0.1 and 20 nJ is observed for fixed repetition rate and number of round trips. In the envisaged single-energy regime $\mathbf{S_2}$ beyond the final bifurcation point BP_{final}, the dependence on seed energy is different [9] as shown in Fig. 4c for 2 kHz repetition rate and 24 round trips. When increasing the seed energy the final bifurcation point BP_{final} is reached at lower pump power, connected with a lower saturation level. With respect to the available pump power of 50 W of our system, a seed pulse energy >20 nJ is required to reach the saturated single-energy regime $\mathbf{S_2}$ yet at the expense of a reduced pulse energy of ~5 mJ compared to lower seed pulse energy.

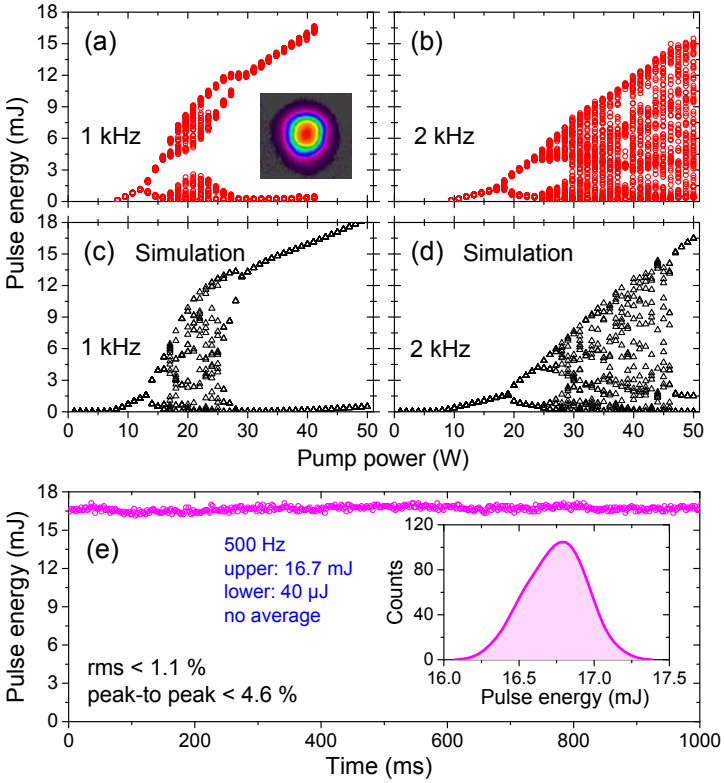

Fig. 5. Characterization of the Ho:YLF RA pulse train dynamics at 1 and 2 kHz repetition rate (24 round trips, stretcher: CVBG). (a,b) Measured bifurcation diagram vs. pump power. Inset (a): Far-field beam profile. (c,d) The same systems simulated, taking into account the observed increase of mode diameters. (e) Pulse-to-pulse stability measurement at 1 kHz in the period-doubling region $\mathbf{P_3}$ for 41 W pump power, recorded for the high-energy pulse train at 500 Hz. Inset: Histogram of the energy-calibrated photodiode signals.

The same scenario is shown in Fig. 4d for the variation of the round trip number for 2 nJ seed pulse energy and 2 kHz repetition rate. At increased round trip numbers, the saturated single-energy region $\mathbf{S_2}$ beyond the final bifurcation point BP_{final} is reached at lower pump power, again at the price of a lower energy saturation level. A further drawback of the increased round trip number is the accumulated B-integral, which prevents pulse compression to Fourier-limited duration after amplification. Taking into account the maximum available pump power of 50 W, the desired saturated single-pulse regime is expected for >26 round trips. At 1 kHz repetition rate, overcoming the multi-stability region should be possible with our RA as BP_{final} is expected at around 30 W pump power for nearly the same number of round trips (Fig. 4a).

A more detailed study of the emission behavior of our 2 µm RA is conducted with the aim of stable emission at higher pulse energies and at few-kHz repetition rates. In such measurements, the seed pulses are stretched to ~950 ps with the help of the CVBG (cf. Fig. 1). Experimental results for repetition rates of 1 and 2 kHz are presented in Figs. 5a and 5b where the distribution of RA pulse energies is plotted as a function of incident pump power. The data were recorded with increasing the pump power in steps of 1 W and detecting 100 emitted pulses at each step with the energy-calibrated photodiode mentioned above. The amplification thresholds are at ~7 W pump power in both cases. The following region of linear increase of single-pulse energy with pump power ends at 12 W and 17 W for 1 and 2 kHz repetition rate, respectively. After the first bifurcation point period-doubling starts. In each branch the second bifurcation point is then reached at 16 W and 25 W for 1 and 2 kHz, respectively, leading to chaotic looking behavior above these values. While at 1 kHz the chaotic region turns into a stable periodic-doubling regime above 28 W pump power, at 2 kHz the chaotic behavior remains up to the maximum applied pump power of 50 W.

The experimental results display some similarity with the simulations of Fig. 4 but do not agree in a quantitative way. An important deviation from our model is the continuous increase of the maximum pulse energy with pump power beyond the expected saturation level. In our experimental pumping geometry, we observe a slight increase of the pump mode diameter with pump power and attribute the associated increase of the emitted pulse energy and the saturation level to the effect of negative thermal lensing in Ho:YLF [15]. Under intense end-pumping in the ring cavity, in turn, the laser mode size in the crystal increases due to the negative thermal lens. Our resonator is stable up to a negative thermal lens around 350 mm which corresponds to a 15% mode size increase. Apparently, the unwanted increase of the pump mode matches the increased laser mode well, both associated to pump power scaling.

As a next step, the RA mode extensions are included into our model. As shown in Figs. 4c and d, the simulation results based on the improved model are in good agreement with the experimental behavior of the Ho:YLF RA (Figs. 5a and b). The saturation level of the RA is reached at a pulse energy of about 12 mJ corresponding to 25 W pump power at 1 kHz and grows with further pump power scaling because of the associated mode increase (Fig. 5c). A benefit of the increasing saturation level is a higher amplified pulse energy. However, the single-energy regime $\mathbf{S_2}$ of the RA which is expected above 30 W pump power at a 1 kHz repetition rate for constant mode diameters (Fig. 4a) is no longer accessible. Operating at a constant pump mode diameter with increasing pump power would require an active concomitant re-adjustment of the telescope in the pump beam which is beyond the present experiments.

We now consider the 1 kHz RA in the range beyond 30 W pump power (Fig. 5a). Up to 42 W pump power, the emitted pulse energy in the upper bifurcation branch increases from 12 to 16.7 mJ whereas the pulse energy in the lower bifurcation arm remains nearly unchanged and amounts to 40 µJ only. We analyze the pulse energy dynamics with a fast photodiode. 1000 consecutive pulses were recorded within a time window of 1 s. The energy values of the 500 pulses in the high gain amplification branch are plotted in Fig. 5e for 41 W pump power. We observe a high stability of the resulting 500 Hz pulse train with a pulse-to-pulse rms variation <1.1% and peak-to-peak fluctuations <4.6%.

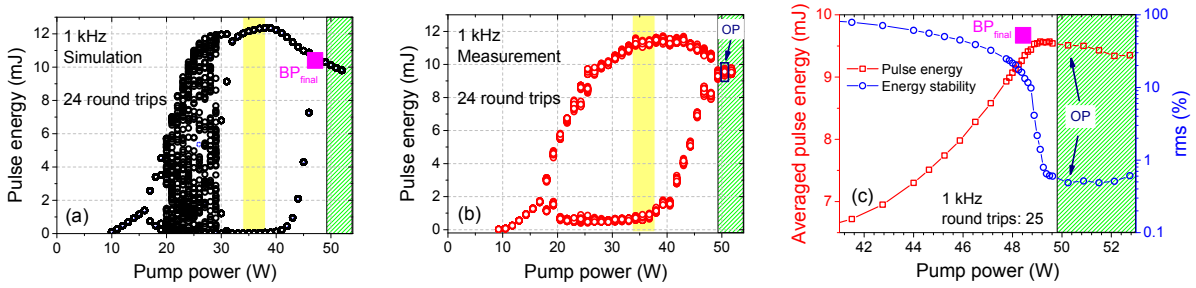

Fig. 6. (a) Simulated and (b) measured Ho:YLF RA bifurcation diagram at 1 kHz repetition rate and 24 round trips indicating the range of stable double-pulsing (yellow coded bar) and the single-energy regime (green coded bar). (c) Averaged pulse energy and pulse-to-pulse stability of the Ho:YLF RA operating at 1 kHz repetition rate below BP_{final} and beyond in the single-energy regime (BP_{final}: final bifurcation point; OP: operation point.

Next, we identify the conditions for the transition in the single-energy regime at 1 kHz pulse repetition rate for a maximum pump power of 50 W. Figure 6(a) shows the simulated bifurcation diagram of our Ho:YLF RA at a 1 kHz repetition rate and 24 round trips indicating the most interesting operation regimes, i.e., stable double-pulsing (yellow coded bar) and the single-energy regime (green coded bar) beyond the final bifurcation point (BP_{final}). Based on our model we slightly re-designed the RA compared to our previous setup with respect to mode matching, aiming at operation in the single-energy regime beyond BP_{final} and at the available pump power of ~55 W. The measured complete RA bifurcation diagram of the re-designed RA at 1 kHz and 24 round trips is presented in Fig. 6(b). It agrees well with our numerical simulations [Fig. 6(a)]. Only the predicted multi-pulsing between 20 and 30 W pump

power is less pronounced in the experiment. The highest pulse energy of 12 mJ can be extracted in the stable double-pulsing regime in the upper bifurcation branch (yellow coded bar), however at 0.5 kHz, the half of the repetition rate. BP_{final} appears at a pump power of 47 W and denotes the transition to the single-energy regime where any multi-stabilities and chaotic behavior have been overcome. The extracted RA pulse energy of 9.7 mJ is the by far highest reported for 2-µm RAs operating in the single-energy regime [16,17]. Performing the transition to the single-energy regime, the RA's pulse-to-pulse stability is further improved with a rms value <0.5% as recorded both by a fast photodiode and energy meter. Figure 6(c) shows the corresponding pulse stability measurement in the vicinity of BP_{final} and beyond in the single-energy regime (green coded bar). Gain narrowing in the RA reduces the spectral bandwidth and the pulse duration to 2.5 nm and 250 ps, respectively.

To summarize this chapter, nonlinear dynamics of cw pumped regenerative amplifiers operating at 2 µm are investigated theoretically and experimentally. At repetition rates near 1 kHz, three different operation regimes are observed, including stable regular, chaotic, and subharmonic dynamics. The measured bifurcation diagrams of the cw-pumped RA emission agree well with our simulations. Exploiting a narrow parameter window beyond the onset of chaos enables operation of a high-gain picosecond Ho:YLF regenerative amplifier which delivers up to 16 mJ picosecond pulses at 0.5 kHz in the stable periodic-doubling regime. The modeling of the instabilities of our RA successfully predicted the transition in the stable single-energy operation in the saturated regime at the aimed 1 kHz repetition rate with a pulse energy of 10 mJ.

2.4 Power amplification and compression of the picosecond 2-µm pump pulses

For further amplification two single-rod booster amplifiers are utilized in single-pass geometry with longitudinal pumping (Fig. 10). The pump power for the amplifiers are provided by cw Tm:fiber lasers (IPG Photonics), identical to the pump laser for the RA. Due to the nearly diffraction-limited beam quality of the pump lasers excellent overlap between pump and amplified beams are provided. The pump spot is chosen comparably large to avoid any damage to the Ho:YLF crystal. To minimize adverse effects of water vapor absorption on the pump beam and the generated 2-µm pulses, both amplifiers are purged with nitrogen.

After mode-matching by a lens arrangement, the ~10 mJ pulses from the RA are sent to the first booster amplifier featuring a 0.75%-doped 50 mm long Ho:YLF rod as the gain medium. The available cw pump power amounts to 105 W. Figure 7 shows the measured pulse energy vs. pump power for the two consecutive booster amplifiers at 1 kHz repetition rate. At the maximum pump power of ~105 W the output of the first single-pass amplifier is 33 mJ (Fig. 7(a)). The beam quality after the first booster is nearly unaffected by the amplification process with the measured M^2 better than 1.2 (inset, Fig. 7(a)).

The pulses are mode-matched and then sent to the second booster amplifier for further amplification. The design of this amplifier is identical to the first one but the Tm:fiber laser pump source delivers a higher power of 120 W. The maximum energy after the second single-pass Ho:YLF amplifier is further linearly scaled up to 55 mJ corresponding to an average power of 55 W (Fig. 7(b)). The extraction efficiency for the whole Ho:YLF amplifier chain is sizeable 20.4% and the single pass gain of the two power amplifiers amounts to 5.8. The peak intensity in both power amplifiers is kept slightly below 7 GW/cm^2 because damage of the Ho:YLF AR-coatings is detected above this value.

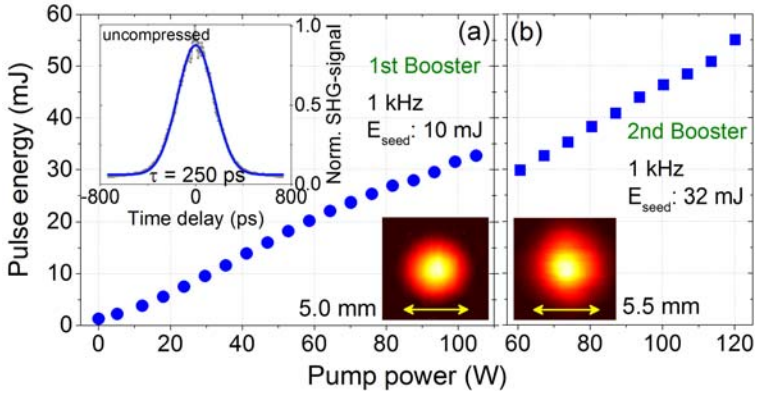

Fig. 7. Dependence of amplified pulse energy on pump power of the two subsequent Ho:YLF booster amplifiers at 1 kHz repetition rate. (a) First booster amplifier (insets: Far-field intensity distribution and autocorrelation trace). (b) Second booster amplifier (inset: Far-field intensity distribution).

Due to the different dn/dT in the birefringent Ho:YLF crystal, the beam profile after the second amplifier displays a slight astigmatism. Therefore, the crystal of the second amplifier is rotated by 90° with respect to the first amplifier rod. To preserve maximum amplification around 2050 nm in the π-polarization of Ho:YLF a half-wave plate is placed between the power amplifiers. In this way the astigmatism is compensated and the excellent beam profile after the first booster amplifier is preserved as shown in the insets of Fig. 7(b). The pulse energy vs. pump power dependences are linear, indicating no detrimental thermal effects for both of the directly water-cooled amplifiers (Fig. 7). To minimize harmful effects of water vapor absorption on the pump beam and the generated 2-µm pulses, the RA and both booster amplifiers are purged with nitrogen.

The long term stability of the complete Ho:YLF amplifier system for more than one hour was characterized with the same techniques as for the RA and is presented in Fig. 8. About 60 minutes are required to reach the thermal equilibrium accompanied by a slight pulse energy drop of ~4%. For reasons of time exposure, the presented results of the RA in Fig. 6 and of the two booster amplifiers in Fig. 7 were recorded without attaining the full thermal equilibrium of the amplifiers at each data point. The characterization of the pulse-to-pulse stability after the setting time of the complete system reveals a superior performance and amounts to <0.3% rms. The slightly larger rms value after the first booster amplifier of <0.5% compared to that after the second booster amplifier of <0.3% is due to the similar absolute variance of the pulse-to-pulse fluctuations of both.

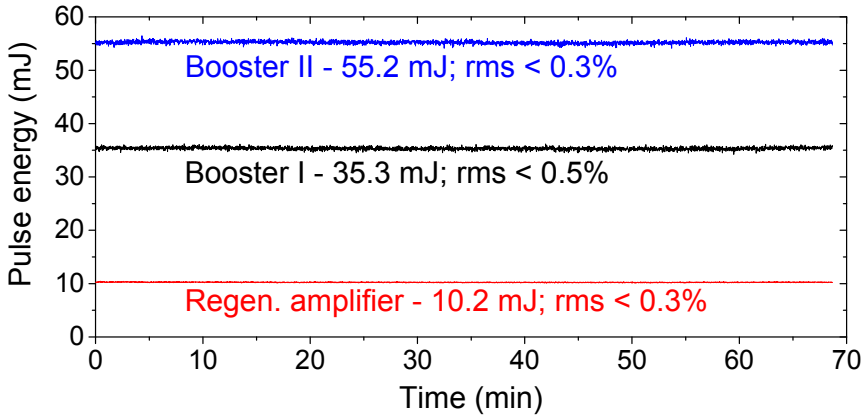

Fig. 8. Long term pulse stability measurement of the Ho:YLF regenerative amplifier and the two subsequent Ho:YLF power amplifiers.

For pulse recompression, two identical large-aperture CVBGs (10 x 10 mm^2) with a dispersion of 39 ps/nm are applied in sequential order. Absorption of the 2 µm pulses in the PTR glass

heats the CVBGs and can result in thermal beam distortions at average power levels beyond 50 W. We implemented an arrangement of two CVBGs to avoid double passage and, thus, stronger heating of a single CVBG. The few percent absorption leads to a notable thermal load in the 50 mm long CVBGs, which immediately affect its dispersion via a thermal wavelength shift of 7 pm/K [18]. After passage through the first compressor CVBG, the pulses are moderately compressed to a duration of 78 ps as measured by a commercial autocorrelator (APE). The resulting intensity of the 50 mJ pulses is 3 GW/cm^2.

The recorded optical spectrum of the compressed pulse after the second CVBG is shown as an inset in Fig. 9. The spectrum is centered at 2050 nm and exhibits a FWHM of 1.8 nm, slightly reduced by further gain narrowing in the power amplifiers. The spectrum is well fitted by a Gaussian with some additional modulation due to several weak satellite pulses. The final spectral width supports a ~3.5 ps Fourier-transform limited pulse. For optimum compression, the resulting pulse intensity exceeds 60 GW/cm^2, 20 times higher than the maximum value reported for pulse compression with CVBGs at 2 µm [5]. Nevertheless, to avoid the risk of optical damage, we limited the pulse energy in the second CVBG to ~28 mJ, which results in a compressed output energy of 25 mJ. The total throughput of the compression assembly containing the two CVBGs was 81%. The residual absorption in the CVBGs at 2 µm represents a challenge for further up-scaling the average output power and may require other compressor schemes, e.g., a grating compressor of the Treacy type.

The autocorrelation (AC) trace measured after the second compressor CVBG is shown in Fig. 9. The black dots represent the measured AC trace, with a FWHM of 6.5 ps. Assuming a Gaussian pulse shape (red curve), we deduce a duration of 4.3 ps, fitting only to the central pulse. The time-bandwidth product has a value of 0.56, only 28% above the Fourier limit. Analysis of the AC trace reveals that the main pulse is accompanied by a number of weak satellites. The strongest of these satellites appears at 8 ps delay and carries about 8.5% of the energy. This satellite is mainly responsible for the modulation in the spectra. All other satellites together carry a similar amount of energy, and the energy content of the main pulse is estimated as 85%. In Ref. [9], 11-ps pulses were reported in the same pulse energy range, using a CVBG with larger aperture of 25 x 27 mm^2. From an analysis of the AC in [5], we deduce a satellite energy content of 32%. i.e., more than twice our value. In both cases, the exact source of the satellite pulses is unclear. We suspect that spurious birefringent filter effects either in the Ho:YLF rods or in the Pockels cell of the RA are a possible explanation for the emergence of the satellites. Accounting for the satellite content, we estimate a peak power of our pulses of 4.4 GW, most probably a new record value for millijoule pulses in the 2 µm wavelength range.

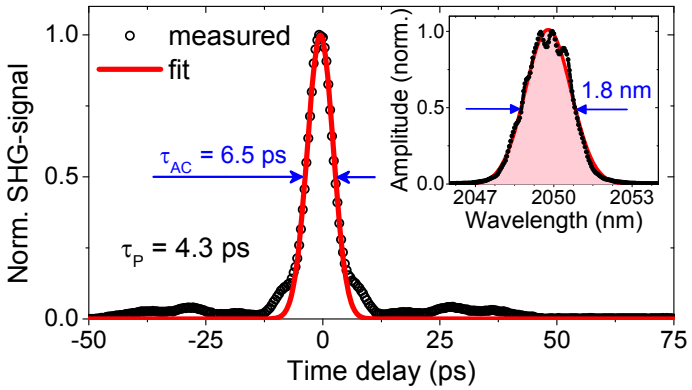

Fig. 9. Autocorrelation trace and optical spectrum (inset) of the compressed pulse after the Ho:YLF booster amplifiers with an energy of 25 mJ.

The excellent pulse characteristics are achieved despite the slight dispersion mismatch of stretcher and compressor CVBGs which would not ensure temporal reciprocity between pulse stretching and compression. The dispersion of all CVBGs was measured with 1 nm spectral

resolution and linearly fitted for its full reflection bandwidth of 11 nm. Taking into account the bandwidth of the emitted pulses with a FWHM of 2-3 nm, the measured CVBG dispersion values can differ slightly in this narrow spectral range. Furthermore, the observed heating of the compressor CVBGs would tend to increase the dispersion. Obviously, these effects contribute to nearly match the stretcher and compressor dispersion and to accommodate for the material GDD of the different amplifiers.

To summarize this chapter, the demonstrated picosecond 2-µm amplification system based on Ho:YLF delivers 55 mJ pulses at a 1 kHz repetition rate, which is to the best of our knowledge the highest pulse energy reported for kHz CPA systems at 2 µm. The system, operating at room temperature, displays an excellent stability with a pulse-to-pulse rms as low as 0.3%. This low noise level mainly originates from the high-gain Ho:YLF RA, which is optimized for stable operation in the single-energy regime. In the 1 kHz pulse train, ~10 mJ pulses were generated, the highest energy to date of any single-energy picosecond RA emitting around 2 µm. Seeding the two subsequent single-pass booster amplifiers a single pass gain of 5.8 was achieved resulting in 55 W average power. This value corresponds to a high extraction efficiency for the whole amplifier system beyond 20% with respect to the optical pump power. Pulse compression at 25 mJ pulse energy provides almost transform-limited pulses with a duration of 4.3 ps, translating into the highest peak power of 4.4 GW achieved for 2-µm CPA systems so far.

2.5 High-energy, femtosecond Optical Parametric Chirped Pulse Amplifier at 5 µm

The layout of our mid-IR OPCPA source is presented in Fig. 10. The already described seed source (chapter 2.1) is operating at 40 MHz. This three-color laser system emits synchronized femtosecond pulses at 1.0 µm (16 mW), 1.5 µm (350 mW) and 2.0 µm (35 mW). The seed for the OPCPA is generated through difference-frequency generation (DFG) of the femtosecond pulses of the front-end, ensuring large bandwidths in the mid-IR [19]. The signal pulse is generated at 3.4 µm via DFG between the 1.0 and 1.5 µm pulses in a 1 mm long fan-out periodically poled lithium niobate crystal (MgO:PPLN). DFG yields 30 pJ pulses with a duration of 25 fs and a spectrum covering 700 nm bandwidth (FWHM) (Fig. 11a).

The 2-µm CPA system, described in chapter 4, is used as pump source operating at 1 kHz. To prevent nonlinear effects and thermal problems in the available CVBGs we limited the pulse energy for compression to 25 mJ. Using one highly-dispersive CVBG (compression factor: 77 ps/nm) the pulses are moderately compressed to a duration of 30 ps. The second installed compressor scheme, a design containing two CVBGs with adapted dispersion, see chapter 2.4, provides shorter pulses with a duration of 4.3 ps.

The vast majority of OPCPA systems employ gratings to compress pulses after amplification. They offer large dispersion, allow exact compensation of grating stretcher induced dispersion terms and setup induced material dispersion can be compensated to a certain amount. Unfortunately, even specially designed broadband grating compressors offer a maximal transmission of <80%. In our target setup, this would reduce the generated idler pulse energy significantly. In contrast, bulk material compressors with an appropriate antireflection coating are nearly lossless. Their main drawback is the rather large, always positive third order dispersion (TOD), which has to be compensated by additional elements such as prisms, chirped mirrors or spatial light modulators.

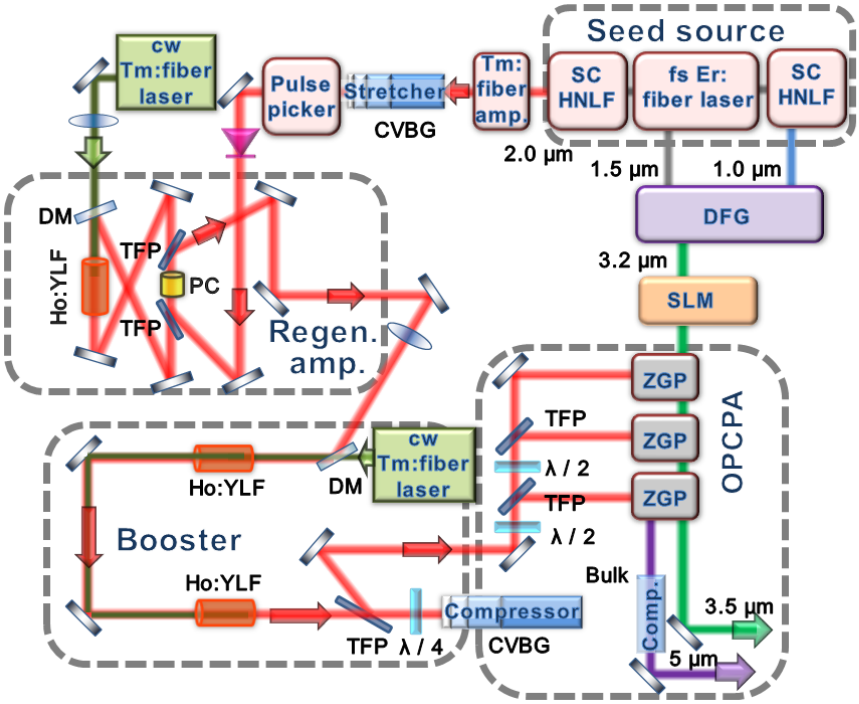

Fig. 10. Setup of the mid-IR OPCPA source pumped at 2 µm. The main parts are the seed source, the difference frequency generation (DFG), the 2-µm Ho:YFL CPA amplifiers and the three OPA stages based on ZGP crystals. RA, regenerative amplifier; Booster, power amplifier; CVBG, chirped volume Bragg grating; SC, supercontinuum gen.; HNLF, highly nonlinear fiber; PC, Pockels cell.

The optical parametric amplification chain is composed of three stages, designed for different gain levels (Fig. 10). We chose ZGP crystals (BAE Systems), the most promising nonlinear material for 2-µm pumped OPCPA, which features an extremely high nonlinearity of d_{eff} = 75 pm/V [1]. In the first two OPA stages a noncollinear geometry is applied ensuring broadband phase-matching. Both contain AR-coated ZGP crystals with 5 x 5 mm^2 aperture (type-I, noncollinear angle: 2.0°, θ = 58.6°). The optimal pump to seed pulse duration is gain dependent. Since the gain differs greatly in a multi-stage OPA, the seed pulse duration has to be adapted accordingly for each stage for optimal conversion efficiency and bandwidth. The spectral gain narrowing, which is primarily due to the high-gain first OPCPA stage can be minimized by choosing a small signal-to-pump pulse duration ratio. For the subsequent low-gain stages the extraction efficiency is optimized by increasing the signal-to-pump pulse duration ratio. Taking into account the intended gain levels for the three OPA stages the signal pulses are stretched to 8 ps and 18 ps in front of the first and second stage, respectively, using AR-coated sapphire rods.

Seeded by the negatively chirped signal pulses and focusing the ~0.5 mJ pump to an intensity of 2 GW/cm^2 the first stage provided a gain >10^5 and spectrum as broad as the DFG without signs of gain narrowing (Fig. 11a, blue line). The 9-µJ signal pulses are then further stretched, as already described, to increase the conversion efficiency in the following OPA stages. Pumped by 2.2 mJ and similar pump intensity as in the first stage which is close to the damage threshold of ZGP, the second amplifier yields 270 µJ signal pulses. The corresponding spectrum is centered at 3.4 µm with a bandwidth of 500 nm (FWHM) indicating slight saturation as shown in Fig. 2a (green line). We are not aiming at excessive saturation to keep the Strehl ratio high for application experiments. In the final stage a ZGP crystal (type-I, θ = 56°) with a larger aperture of 10 x 10 mm^2 and 2 mm thickness is employed and a collinear OPA design is chosen to prevent an angular dispersed idler. To avoid damage of the ZGP crystals only 12 mJ of the available 2 µm pulse energy is applied in the final OPA stage resulting in 1.3 mJ per pulse in the idler, the highest energy so far in the mid-IR. We achieved a noticeable energy conversion efficiency of >10% from the pump to the idler which is in good

agreement with theoretical simulations of the frequency conversion process. For the simulation of the OPA process we used a nonlinear propagation code [20].

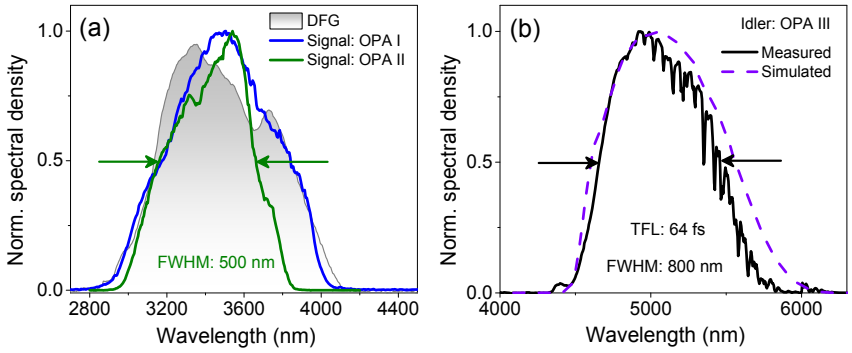

Fig. 11. Characterization of the OPCPA performance (without SLM). (a) DFG spectrum (grey), signal spectrum after the 1st (blue) and 2nd OPA stage (green), (b) idler spectrum after the 3rd OPA stage measured (black) and calculated (purple) (TFL: Fourier-transform limited).

Given the 1 kHz repetition rate of the OPCPA system a sizeable average power of 1.3 W is achieved. By blocking the signal of the OPA chain we estimate the contribution of superfluorescence to below 5%. The signal pulses at 3.4 µm with energy of 2.2 mJ are filtered out by dichroic optics. The OPCPA output spectrum of the idler centered at 5.1 µm is recorded with an imaging spectrometer equipped with a cooled MCT detector and shown in Fig. 11b. The 800 nm broad (FWHM) spectrum supports a Fourier-transform limited (TFL) pulse duration of 64 fs. The small dips and the deviation with our simulation at the red edge of the spectrum are ascribed to water vapor absorption because the OPA stages are not purged.

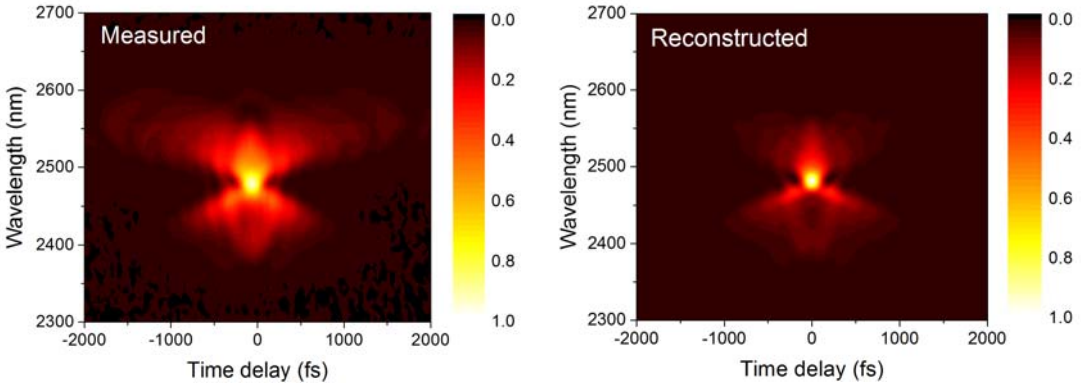

Fig. 12. Characterization of the compressed 5 µm pulses. Measured and reconstructed second harmonic generation frequency resolved optical gating (SHG-FROG) traces.

In a first series of experiments, the compression of the positively chirped idler pulses is performed with 400 mm long CaF_2 bulk material, adjusted to compensate the introduced GDD. The compressed pulses are characterized by recording second harmonic generation frequency resolved optical gating (SHG-FROG) traces, see Fig. 12, which yields a pulse duration of 160 fs (FWHM) corresponding to a sub-ten optical cycle signature (Fig. 13a). The retrieved pulse shape with the distinct post-pulse structure indicates a fairly large amount of uncompensated third-order dispersion (TOD) but also higher orders (Fig. 13a). During parametric amplification, the generated idler exhibits a reversed sign of GDD relative to the signal, while the TOD does not invert the sign. Since our OPA stages are not purged the humidity in air also contributes to the TOD. Our simulation of the pulse shape (Fig. 13a, grey line) agrees well with the measurement and confirms the high amount of remaining TOD (~2 x 10^6 fs^3). The latter cannot be compensated by adding further pertinent bulk material in the stretcher or compressor, because of their always positive TOD (Fig. 14). The compensation of the residual TOD and higher order dispersions will be performed in a next step by implementing a spatial light modulator in the OPCPA system. Nonetheless, the main peak contains 66% of the pulse energy which corresponds to

a sizable peak power of 5.3 GW. The nearly diffraction-limited Gaussian far-field intensity distribution and the excellent stability of the recompressed pulses at the 1 kHz repetition rate with an rms of 1.3% for a duration of one hour are presented in Fig. 13b. The results represent the first femtosecond OPCPA at λ>4 µm at millijoule pulse level. Also with respect to pulse duration and stability the 5 µm OPCPA outperforms competing systems [21].

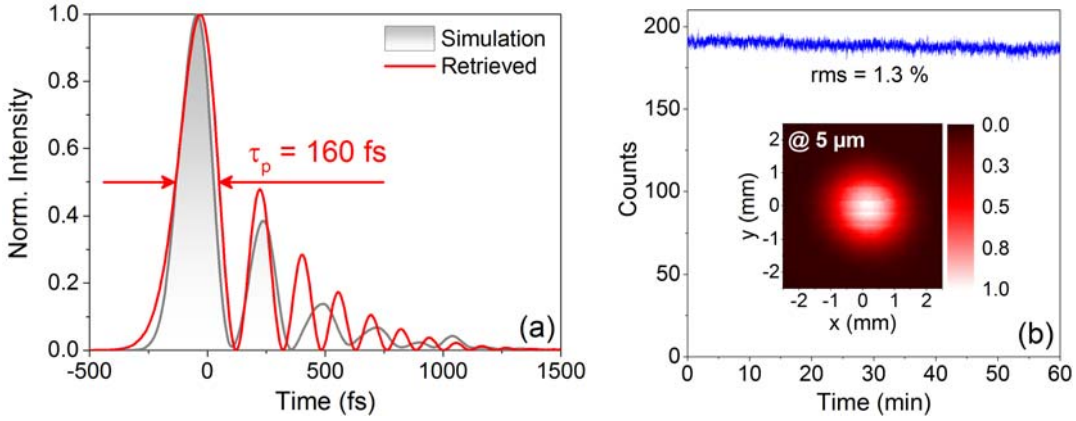

Fig. 13. Performance of the 5 µm idler pulses. (a) SHG-FROG characterization of the compressed pulses, retrieved temporal pulse shape (red line) and simulated pulse shape (grey line); (b) Long-term pulse stability measurement, Inset: Far-field intensity distribution.

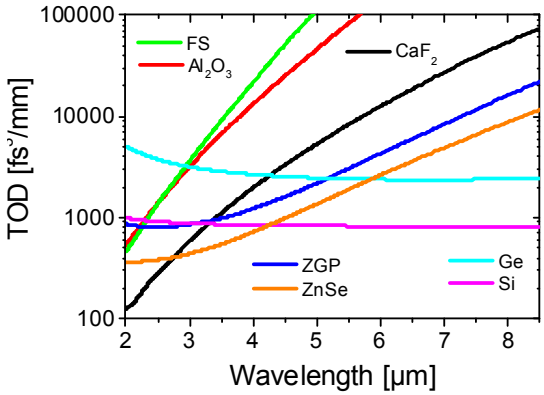

Fig. 14. Third-order dispersion (TOD) of pertinent mid-IR materials.

To summarize this chapter, we have demonstrated a 5-µm optical parametric chirped pulse amplification (OPCPA) system delivering multi-GW femtosecond pulses at a 1 kHz repetition rate. The system is pumped by the developed highly stable ps 2-µm CPA system to exploit the high nonlinearity of $ZnGeP_2$ crystals for parametric amplification. In the 1 kHz pulse train, up to 1.3 mJ idler pulses were generated and compressed to 160 fs duration by dispersion management based only on bulk materials. This pulse duration corresponds to a sub-ten cycle signature. The pulse energy represents the highest to date of any femtosecond mid-IR source beyond 4 µm. The OPCPA is characterized by an excellent stability with a pulse-to-pulse rms as low as 1.3%. This pulse characteristics represents the highest peak power of 5.3 GW achieved for 5-µm OPCPA systems to the best of our knowledge, and, if focused to a 15-µm spot diameter, would reach a peak intensity of ~6 x 10^{15} W/cm^2.

A recent systematic analysis of higher order dispersion in the OPCPA chain and the implementation of a spatial light modulator for minimizing detrimental dispersion effects has allowed for bringing the mid-IR pulse duration down to less than 100 fs with a clean intensity envelope. The output pulse energy under such conditions was 0.65 mJ.

The system appears scalable with respect to repetition rate via a pulse picking rate in the 1 to 10 kHz range and with respect to the mid-IR pulse energy by using ZGP or CSP crystals with a

larger aperture for parametric amplification driven with the full available 2-µm pump energy of 50 mJ.

Presently, the extension of the system towards 50 mJ pump power at 2 µm is being finalized. After optimization of the parameters of the 5-µm pulses generated at this elevated pump power level, the whole setup will be moved to an x-ray laboratory and be combined with an existing source for laser-driven generation of femtosecond hard x-ray pulses in metal targets. An increase in the number of x-ray photons generated per 5-µm driver pulse by a factor of 10 to 100 is anticipated in comparison to existing sources driven by near-infrared pulses.

3. References

[1] V. Petrov, F. Rotermund and F. Noack, “Generation of high-power femtosecond light pulses at 1 kHz in the mid-infrared spectral range between and 12 µm by second-order nonlinear processes in optical crystals”, J. Opt. A: Pure Appl. Opt. **3**, R1-R19 (2001).

[2] M. Grishin, V. Gulbinas, and A. Michailovas, “Dynamics of high repetition rate regenerative amplifiers,” Opt. Express **15**, 9434–9443 (2007).

[3] M. Eichhorn, “Quasi-three-level solid-state lasers in the near and mid infrared based on trivalent rare earth ions,” Appl. Phys. B **93**, 269-316 (2008).

[4] P. Malevich, G. Andriukaitis, T. Flöry, A. J. Verhoef, A. Fernandez, S. Ališauskas, A. Pugžlys, A. Baltuška, L. H. Tan, C. F. Chua, and P. B. Phua, “High energy and average power femtosecond laser for driving mid-infrared optical parametric amplifiers,” Opt. Lett. **38**, 2746 (2013).

[5] M. Hemmer, D. Sánchez, M. Jelínek, Vadim Smirnov, H. Jelinkova, V. Kubeček, and J. Biegert, "2-µm wavelength, high-energy Ho:YLF chirped-pulse amplifier for mid-infrared OPCPA", Opt. Lett. **40**, 451-454 (2015).

[6] A. Dergachev, “High-energy, kHz, picosecond, 2-µm laser pump source for mid-IR nonlinear optical devices”, Proc. SPIE **8599**, 85990B-1 (2013).

[7] P. A. Budni, L. A. Pomeranz, M. L. Lemons, C. A. Miller, J. R. Mosto, and E. P. Chicklis, “Efficient mid-infrared laser using 1.9-µm-pumped Ho:YAG and $ZnGeP_2$ optical parametric oscillators,” JOSA B **17**, 723-728 (2000).

[8] B. M. Walsh, N. P. Barnes, and B. Di Bartolo, “Branching ratios, cross sections, and radiative lifetimes of rare earth ions in solids: application to Tm^{3+} and Ho^{3+} ions in $LiYF_4$,” J. Appl. Phys. **83**, 2772–2787 (1998).

[9] H. Fattahi, A. Schwarz, X. T. Geng, S. Keiber, D. E. Kim, F. Krausz, and N. Karpowicz, “Decoupling chaotic amplification and nonlinear phase in high-energy thin-disk amplifiers for stable OPCPA pumping,” Opt. Express **22**, 31440-31447 (2014).

[10] L. M. Frantz and J. S. Nodvik, “Theory of Pulse Propagation in a Laser Amplifier,” J. Appl. Phys. **34**, 2346-2349 (1963).

[11] M. Schellhorn and A. Hirth, "Modeling of intracavity-pumped quasi-three-level lasers," IEEE J. Quantum Electron. **38**, 1455–1464 (2002).

[12] G. Rustad and K. Stenersen, “Modelling of laser-pumped Tm and Ho lasers accounting for upconversion and ground-state depletion,” IEEE J. Quantum Electron. **32**, 1645 (1996).

[13] W. Koen, C. Bollig, H. Strauss, M. Schellhorn, C. Jacobs, M. J. D. Esser, “Compact fibre-laser-pumped Ho:YLF oscillator-amplifier system, ” Appl. Phys. B **99**, 101-106 (2010).

[14] R. C. Stoneman and L. Esterowitz, “Efficient 1.94-µm Tm:YALO laser,” IEEE J. Sel. Top. Quantum Electron. **1**, 78 (1995).

[15] M. Schellhorn, “A comparison of resonantly pumped Ho:YLF and Ho:LLF lasers in CW and Q-switched operation under identical pump conditions,” Appl. Phys. B **103**, 777–788 (2011).

[16] P. Kroetz, A. Ruehl, G. Chatterjee, A.-L. Calderon, K. Murari, H. Cankaya, P. Li, F. X. Kärtner, I. Hartl, and R. J. D. Miller, “Overcoming bifurcation instability in high-repetition-rate Ho:YLF regenerative amplifiers,” Opt. Lett. **40**, 5427-5430 (2015).

[17] P. Malevich, T. Kanai, H. Hoogland, R. Holzwarth, A. Baltuška, and A. Pugžlys, “Broadband mid-infrared pulses from potassium titanyl arsenate/zinc germanium phosphate optical parametric amplifier pumped by Tm,Ho-fiber-seeded Ho:YAG chirped-pulse amplifier,” Opt. Lett. **41**, 930-933 (2016).

[18] A. Glebov, O. Mokhun, A. Rapaport, S. Vergnole, V. Smirnov, and L. Glebov, “Volume Bragg gratings as ultra-narrow and multiband optical filters,” SPIE **8428**, 84280C-1 (2012).

[19] C. Erny, K. Moutzouris, J. Biegert, D. Kühlke, F. Adler, A. Leitenstorfer, and U. Keller, “Mid-infrared difference-frequency generation of ultrashort pulses tunable between 3.2 and 4.8 μm from a compact fiber source, ” Opt. Lett. **32**, 1138-1140 (2007).

[20] G. Arisholm, “General numerical methods for simulating second-order nonlinear interactions in birefringent media," J. Opt. Soc. Am. B **14**, 2543-2549 (1997).

[21] D. Sanchez, M. Hemmer, M. Baudisch, S. L. Cousin, K. Zawilski, P. Schunemann, O. Chalus, C. Simon-Boisson, and J. Biegert, “7 μm, ultrafast, sub-millijoule-level mid-infrared optical parametric chirped pulse amplifier pumped at 2 μm,” Optica **3**, 147 (2016).

4. Statement about economical viability

Commercial exploitation is expected.

5. Cooperation partners

- University of Tarragona, Spain: Calculations of spectroscopic properties of Ho-doped active laser media.
- University of Pisa, Italy: Measurement of absorption and emission cross sections of Ho-doped laser crystals.
- G. Arisholm, Norwegian Defence Research Establishment, Kjeller, Norway: Supporting the OPA calculation

6. Qualification work resulting from the project

Lorenz von Grafenstein, Ph.D. defense expected in Autumn 2017.

7. Presentation of measures to ensure security and availability of research data

http://intern.mbi-berlin.de/en/organization/good_scientific_practice/rules.html

8. List of publications

- L. von Grafenstein, M. Bock, U. Griebner, and T. Elsaesser, “High-energy, multi-kilohertz, Ho-doped regenerative amplifiers around 2 μm,” Opt. Express **23**, 14744-14752 (2015).
- L. von Grafenstein, M. Bock, G. Steinmeyer, U. Griebner, and T. Elsaesser, “Taming chaos: 16 mJ picosecond Ho:YLF regenerative amplifier with 0.7 kHz repetition rate,” Laser Photon. Rev. **10**, 123-130 (2016).
- L. von Grafenstein, M. Bock, D. Ueberschaer, U. Griebner, and T. Elsaesser, “Picosecond 34 mJ pulses at kHz repetition rates from a Ho:YLF amplifier at 2 μm wavelength,” Opt. Express **23**, 33142-33149 (2015).
- L. von Grafenstein, M. Bock, D. Ueberschaer, U. Griebner, and T. Elsaesser, “Ho:YLF chirped pulse amplification at kilohertz repetition rates - 4.3 ps pulses at 2 μm with GW peak power,” Opt. Lett. **41**, 4668-4671 (2016).
- L. von Grafenstein, M. Bock, U. Griebner, and T. Elsaesser, “600 μJ, 5 μm, 1 kHz Femtosecond Optical Parametric Chirped Pulse Amplifier Pumped at 2 μm,” Advanced Solid-State Lasers 2016, paper 2570418.

- L. von Grafenstein, M. Bock, D. Ueberschaer, K. Zawilski, P. Schunemann, U. Griebner, and T. Elsaesser, “5 μm, few-cycle pulses with multi-GW peak power at a 1 kHz repetition rate,” Optica, submitted.

9. List of press releases

Not applicable.